


Article

A Numerical Simulation of Electrical Resistivity of Fiber-Reinforced Composites, Part 1: Brittle Cementitious Concrete

Alireza Miri ¹, Rojina Ehsani ¹ and Fariborz M. Tehrani ^{2,*} 

¹ Department of Civil and Environmental Engineering, Amirkabir University of Technology, Tehran 15916-34311, Iran; alirezamiri@aut.ac.ir (A.M.); rojinaehsani@aut.ac.ir (R.E.)

² Department of Civil and Geomatics Engineering, California State University, Fresno, CA 93740-8030, USA

* Correspondence: ftehrani@csufresno.edu

Abstract: The durability of concrete has a significant influence on the sustainability and resilience of various infrastructures, including buildings, bridges, roadways, dams, and other applications. Penetration of corrosive agents intensified by exposure to freeze-thaw cycles and the presence of early-age cracks is a common cause of reinforced concrete degradation. Electrical resistivity is a vital physical property of cementitious composites to assess the remained service life of reinforced concrete members subjected to corrosive ions attacks. The application of steel fibers reduces the vulnerability of concrete by limiting crack propagation, but complicates field and laboratory testing due to the random distribution of conductive fibers within the body of the concrete. Numerical simulations facilitate proper modeling of such random distribution to improve the reliability of testing measures. Hence, this paper investigates the influence of fiber reinforcement characteristics on electrical resistivity using multi-physics finite element models. Results examine modeling challenges and include insights on the sensitivity of resistivity measures to fiber reinforcement. Concluding remarks provide expected bias of electrical resistivity in the presence of steel fibers and endeavor to facilitate the development of practical guidelines for assessing the durability of fiber-reinforced concrete members using standard electrical resistivity testing procedures.

Keywords: finite element method; fiber-reinforced composites; electrical resistivity; electrical conductivity; material durability; sustainable development; infrastructure resilience; reinforced concrete



Citation: Miri, A.; Ehsani, R.; Tehrani, F.M. A Numerical Simulation of Electrical Resistivity of Fiber-Reinforced Composites, Part 1: Brittle Cementitious Concrete. *Modelling* **2022**, *3*, 164–176. <https://doi.org/10.3390/modelling3010011>

Academic Editors: Ahmed A. Ibrahim and Aly Said

Received: 27 December 2021

Accepted: 15 March 2022

Published: 17 March 2022

Publisher's Note: MDPI stays neutral with regard to jurisdictional claims in published maps and institutional affiliations.



Copyright: © 2022 by the authors. Licensee MDPI, Basel, Switzerland. This article is an open access article distributed under the terms and conditions of the Creative Commons Attribution (CC BY) license (<https://creativecommons.org/licenses/by/4.0/>).

1. Introduction

Durability and service life of construction materials are vital for achieving sustainable development and infrastructure resilience [1,2]. The application of high-performance materials contributes to these goals by reducing lifecycle energy consumption and emitted greenhouse gases and improving the robustness and redundancy of structural elements [3–5]. Prompt performance assessment concerning sustainability and resilience throughout the infrastructure service life optimizes maintenance and preservation efforts and enhances the resourcefulness of the system [6–8].

1.1. Durability of Cementitious Concrete Composites

Cementitious concrete has widespread applications in various infrastructure systems, including buildings, bridges, roads, dams, and other structures. High energy input and greenhouse gas emissions associated with cement production and the vulnerability of reinforced concrete to corrosive environments emphasize the importance of durability and extended service life of concrete members [9–14]. These characteristics are intensified for exposed concrete members like bridge decks, road pavements, and marine concrete [15–18]. Transport properties of concrete reveal the potential intrusion of corrosive agents like chloride ions through concrete cover and the time required for these ions to reach reinforcing

bars and initiation of the degradation process [19–21]. Standard methods determine the chloride diffusion coefficient for hardened concrete samples in the laboratory [22]. Electrical resistivity is a standard practice to evaluate transport properties of new and existing concrete having an established correlation with the chloride diffusivity [23,24]. Standard methods allow both bulk and surface resistivity measures, where the latter is a viable and fast approach for existing concrete members [25–27]. Further, electrical resistivity is a suitable approach for sensor-based structural health monitoring [28].

1.2. Fiber-Reinforced Concrete

Early-age cracking and other deformations caused by structural and environmental loadings accelerate the degradation of concrete in such exposed conditions. Hence, common strategies to extend the service life of concrete focus on controlling crack propagation and limiting the transportation of corrosive agents within the concrete body [29,30]. Fiber reinforcement is an effective technique to mitigate cracking in plain and reinforced concrete members [30–33]. In addition, randomly dispersed fibers contribute to ductility, toughness, stiffness, and strength of concrete elements [30,34–40]. However, the conductivity of steel fibers complicates electrical resistivity measurements. Existing literature indicates that increasing the steel and carbon fiber contents reduces electrical resistivity [40–42]. The fiber content influences the workability of the fresh mixture and hence, is limited to practical ranges often presented as volumetric contents [43]. Correlating these changes results in proposed adjustment factors as a function of fiber reinforcement characteristics, like aspect ratio and volumetric content [42,44–46]:

$$r = e^{(al^2+bl+c)v}, \quad (1)$$

where r is the ratio of the measured electrical resistivity ($\Omega \cdot m$) of fiber-reinforced to plain concrete, l is the fiber length (mm), v is the volumetric fiber content (%), and a , b , and c are regression constants.

1.3. Literature Review

Existing literature is rich in applying steel fiber-reinforced concrete to improve mechanical properties of concrete, including toughness and tensile strength [30]. These applications include the benefits of steel fibers in enhancing concrete conductivity for deicing purposes [47]. Fiber reinforcement may involve adding carbon and graphite powder to achieve the desired electrical resistance [43]. A typical mixture proportioning involves small volumetric quantities of steel fibers, say 1.5%, and more significant proportions of carbon and graphite products, like 25%, to control the workability and consistency of the concrete mixture [43,48]. Experimental investigations have demonstrated the positive effect of steel and carbon fibers on the electrical conductivity at practical volumetric ratios, like 3%, for mono and hybrid fiber applications [49]. However, You et al. (2017) has concluded that the electrical resistivity of concrete is sensitive to variations of fiber content, material, and dimension, considering the broad range of applied fibers in various scales from nano to macro. In addition, the effect of fibers on mechanical properties of concrete, like compressive strength, is vital for engineering applications [50]. Figure 1 displays selected observed data indicating fiber contents and measured surface electrical resistivity of the composite cementitious concrete materials (Table 1). The scattered observations warrant numerical studies to understand the trends of electrical resistivity measures concerning fiber type, content, and geometry.

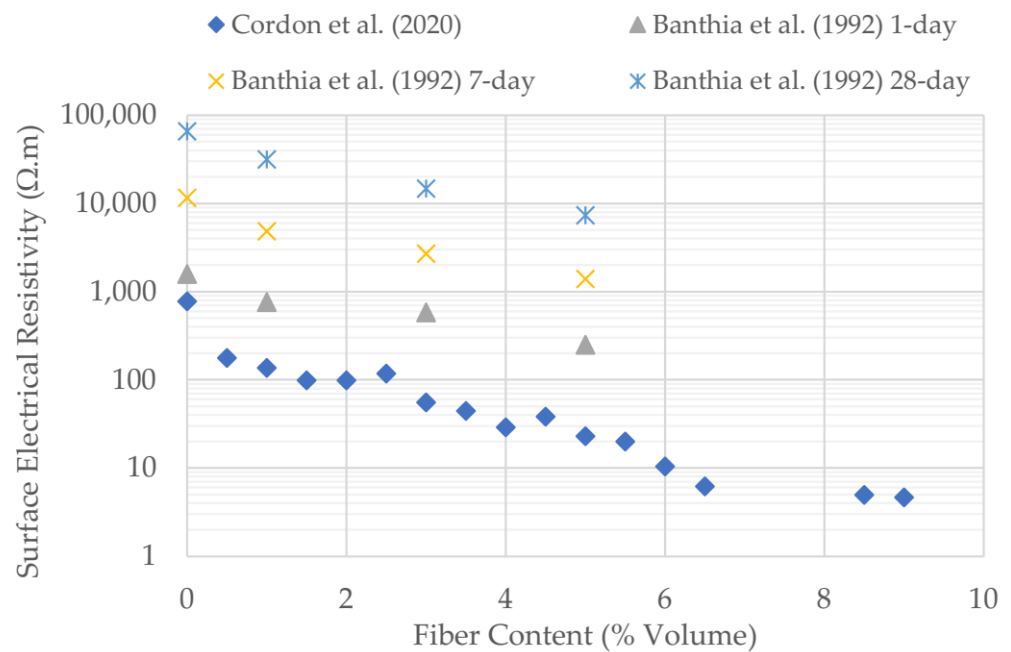


Figure 1. Surface electrical resistivity of selected experimental data [43,49].

Table 1. Selected experimental studies on the electrical resistivity of fiber-reinforced asphalt.

Reference	Matrix	Fibers
Cordon et al. (2020) [43]	Coarse aggregate (S.G. 2.66), fine aggregate (S.G. 2.65), cement type CPV-ARI (S.G. 2.81)	Carbon steel type AII (Tec-Machine), 0.60-mm-diameter, 30-mm-long
Banthia et al. (1992) [49]	Sand–cement ratio of 0.5; silica fume/cement ratio of 0.2	Steel fibers (S.G. 7.85), 25-mm-diameter, 3-mm-long

S.G.: Specific Gravity.

1.4. Significance of the Research

This paper endeavors to address the gap in the knowledge on the viability of surface electrical resistivity testing for steel fiber-reinforced concrete. Existing literature appears to lack information on the feasibility of performing electrical resistivity for steel fiber-reinforced concrete. The significance of this research has roots in the effectiveness of steel fiber reinforcement for enhancing the durability of concrete elements and the practicality of surface electrical resistivity test as an economical means to assess the service life of reinforced concrete. The employed analytical methodology of this research mitigates the inherent uncertainties in the fiber-reinforcement applications and expected bias and precisions associated with the surface electrical resistivity testing. Hence, expected results demonstrate the feasibility and reliability of experimental investigations for existing reinforced concrete elements. Moreover, the presented methodology facilitates a broad parametric study of fiber content and dimensions as an extension and amendment to prior studies with limited parameters.

2. Materials and Methods

The numerical simulation in this research utilizes a multi-physics finite element model powered by COMSOL software (Figure 2) [51–53]. An independently developed program using MATLAB [54] specifies the random dispersion of fibers and determines the location and direction of each fiber as input values for the finite element routine. This program allows customization of fiber dispersion to match desired geometric forms and boundary conditions. Existing studies indicate that the random dispersion of fibers with straight or hooked ends within practical ranges of content and sizes typically follows a uniform

distribution, which is the proposed model for this study [55]. The modeled prototype is a 150-mm cube with an electrical resistivity of $1.0 \times 10^3 \text{ W}\cdot\text{m}$ for the homogenized matrix and $2.4 \times 10^{-7} \text{ W}\cdot\text{m}$ for fibers (Figure 3). The diameter and length of fibers vary with aspect (length to diameter) ratios of 50 (F1) and 25 (F2) (Table 2). The finite element model contains nearly 250 solid objects within the 150-mm cube [44].

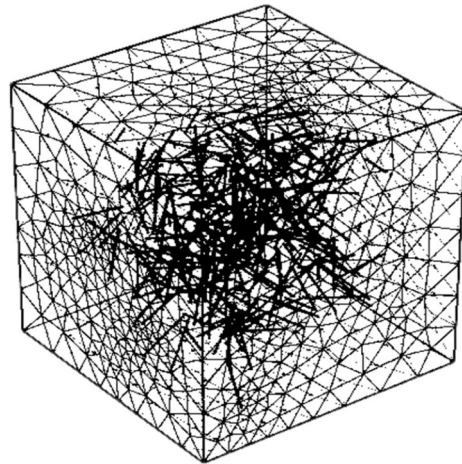


Figure 2. The mesh of a sample finite element model, after [46].

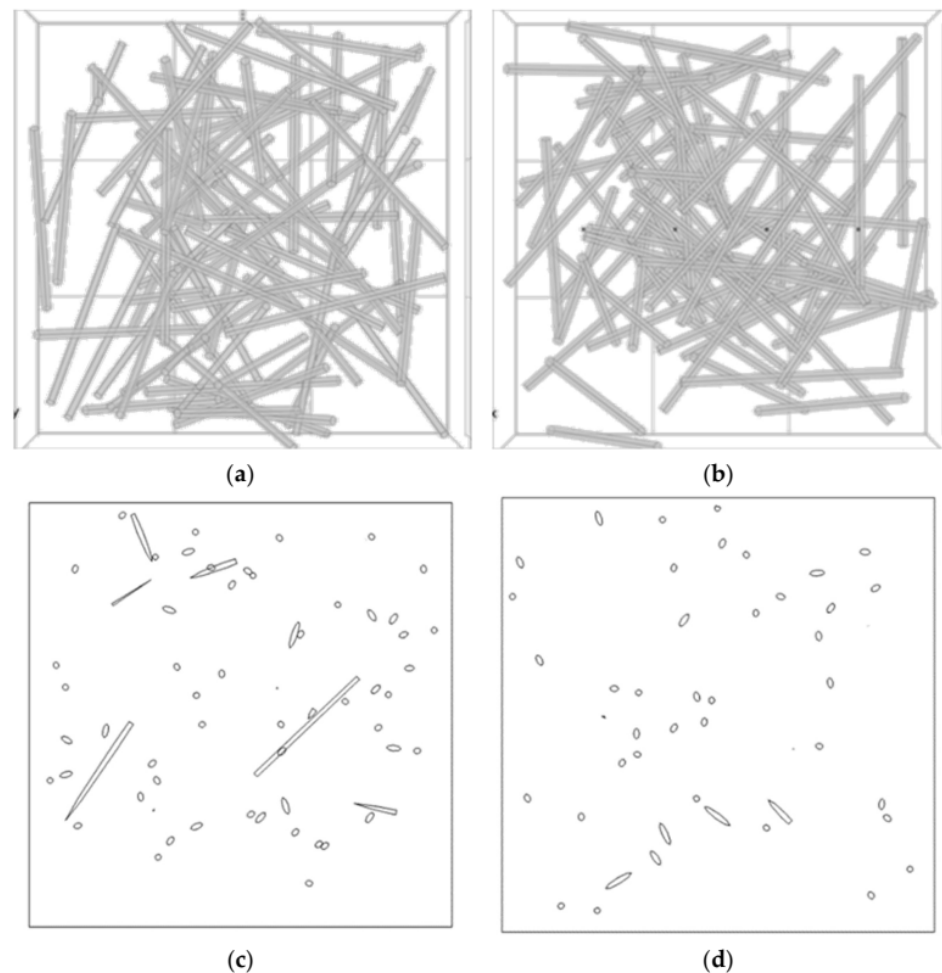


Figure 3. Simulated fiber dispersion from (a) top view, (b) side view, (c) section view at 50-mm height, (d) section view at 100-mm height.

Table 2. Dimensions of fibers.

Model	Length, mm	Diameter, mm
F1-1	25	0.5
F1-2	50	1.0
F1-3	75	1.5
F2-1	50	2.0
F2-2	75	3.0

The model follows Wenner's method using four electrodes at an equal spacing in a row, with two external electrodes transmitting the specified current and two internal electrodes measuring the electrical resistance. Equation (2) expresses the surface electrical resistivity in Wenner's method:

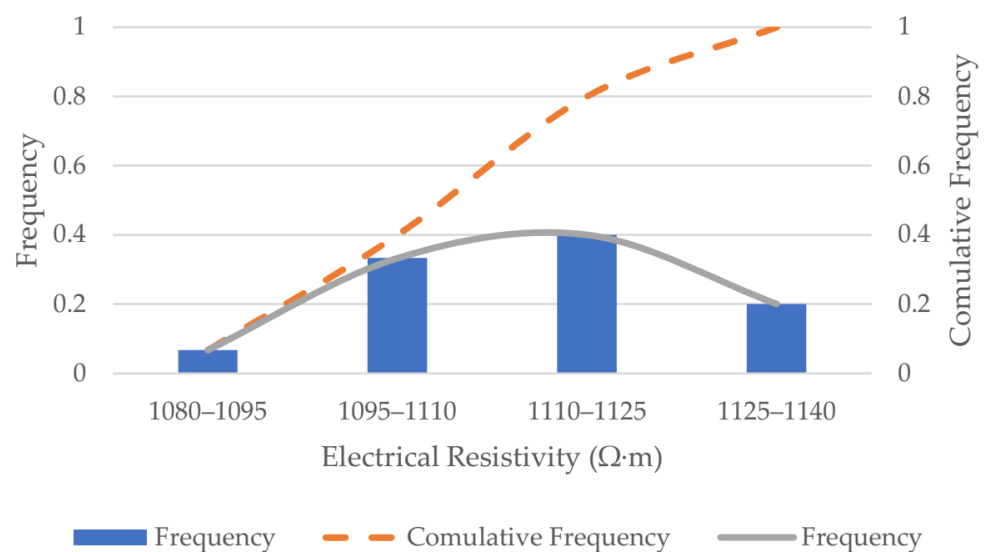
$$\rho = 2\pi sR, \quad (2)$$

where ρ is the surface electrical resistance, R is the electrical resistance, and s is the distance between electrodes. The model imposed a simulated current of 1 A/m^2 at a spacing of 30 mm. The electrical potential formulation follows Poisson's equation combining the Gauss' law and continuity equation:

$$-\nabla \cdot (\sigma \nabla V - J^e) = Q_i, \quad (3)$$

where σ is the electrical conductivity, V is the electric potential, J^e is the volume of external current, and Q_i is the current at the source.

For verification purposes, a total of 15 samples containing 0.025% volumetric content of short fibers were investigated to assure the normal distribution of fibers (Figure 4). Statistical significance levels of normal distribution using Kolmogorov–Smirnov and Shapiro–Wilk tests were 0.2 and 0.563, respectively, both well above the 0.05 threshold indicating a normal distribution. The skewness and kurtosis values were -0.651 and 1.11 , respectively, between an acceptable range of -2 to 2 for a normal distribution [46]. Hence, the random distribution of fibers does not cause specific bias or skew in the numerical results of electrical resistivity.

**Figure 4.** The normal distribution of electric resistivity values for various fiber dispersions, after [46].

Further, parametric studies indicated that changes in clear cover margin within 0, 10, 20, and 30 mm distances from the edge (Figure 5) have a coefficient of variation less than 3.2%, and hence, it has a negligible effect on modeling [46].

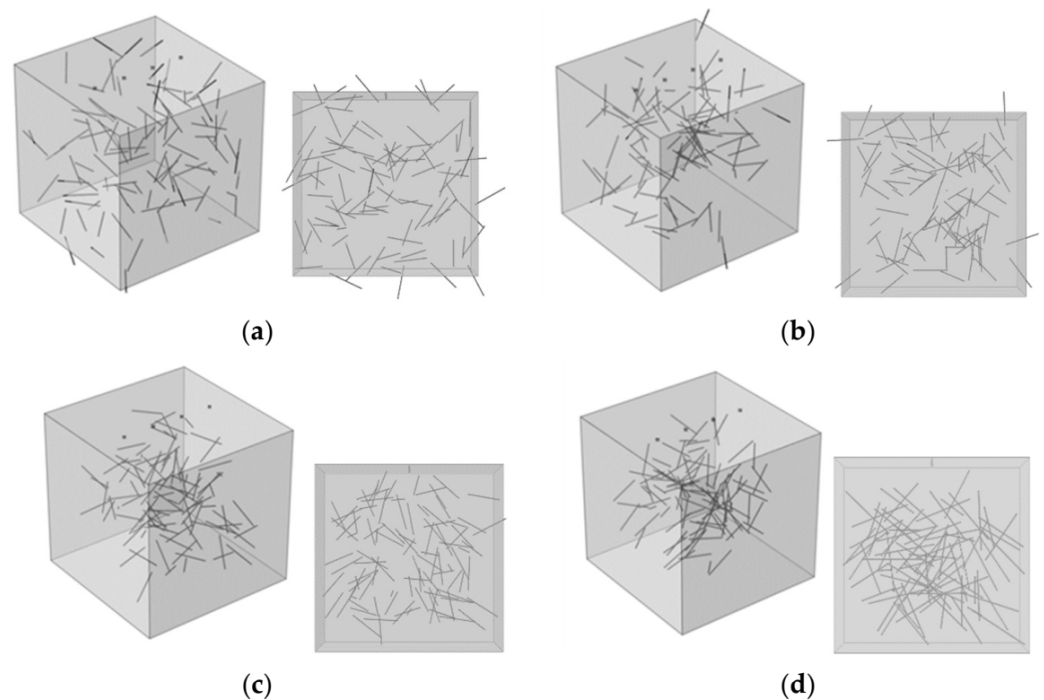


Figure 5. Models with carrying clear margins of (a) 0, (b) 10, (c) 20, and (d) 30 mm, after [46].

3. Results

Electrodes transferring one ampere per square meter are spaced 30 mm at the top surface of the concrete prototype (Figure 6). Red lines mark the passage of electric currents through the concrete body. These lines are concentrated in the presence of fibers due to the meager electrical resistance of the fibers compared to the concrete around them, indicating higher conductivity in those regions (Figure 7). Traced flow lines confirm the physical science understanding that the electrical current is passing through the lowest resistance path disregarding the dispersion of fibers. Hence, deviation of fiber dispersion from a uniform distribution due to gravity forces and hydrostatic pressures at concrete depth does not significantly influence the surface electrical resistivity.

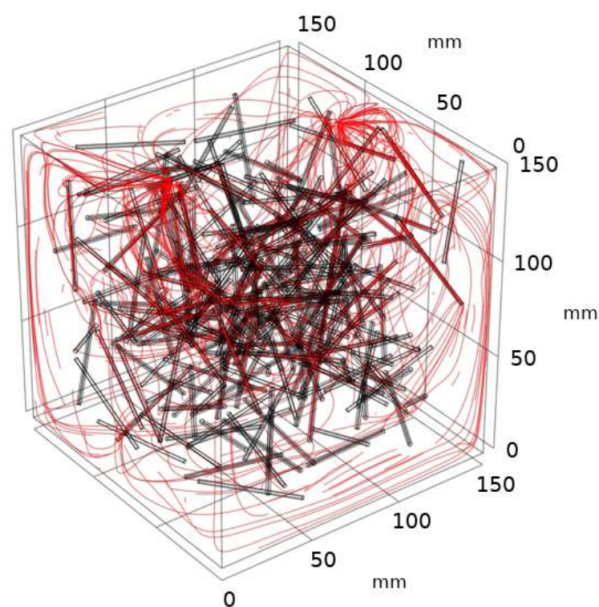


Figure 6. Electrical conductivity lines in the simulated model.

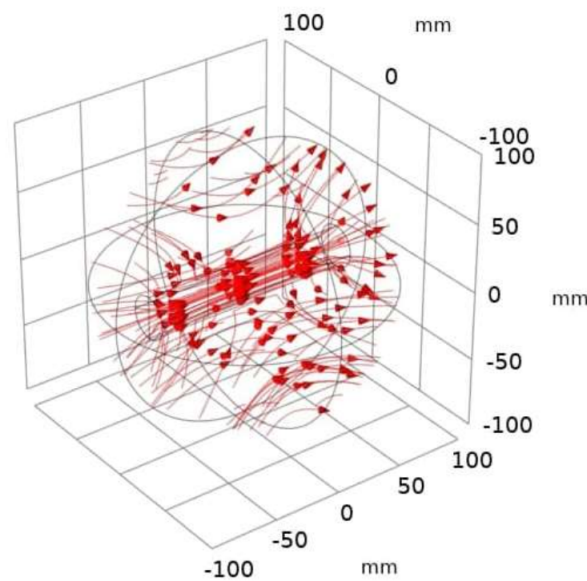


Figure 7. Current density in the proximity of conductive fibers.

An increase in fiber content causes a reduction in calculated surface electrical resistivity (Figure 8). The reduction rate is sensitive to the aspect ratio and the size of fibers (Table 3). Prototype group F1, having a higher aspect ratio than prototype group F2, has higher decline rates in electrical resistivity due to an increase in fiber content. However, the changing trend with fiber size variation is more complex, as fiber size influences the number of fibers. So, it is essential to include multiple variables for a conclusive regressive function.

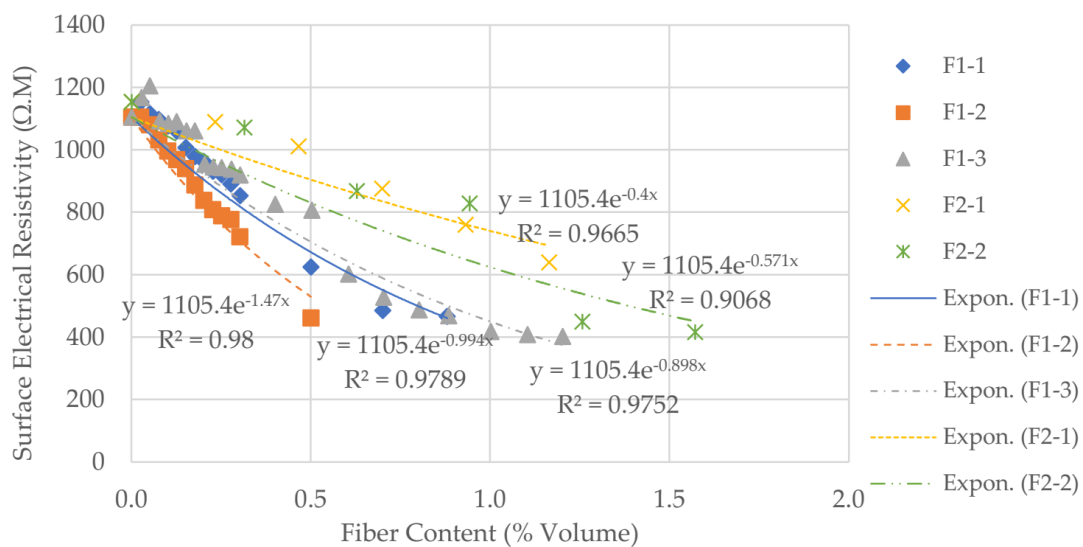


Figure 8. Trends of normalized electrical resistance for different percentages of fiber content.

Table 3. Regression results for surface electrical resistivity.

Model	Exponential Rate of Decline	Coefficient of Determination
F1-1	−0.994	0.9435
F1-2	−1.47	0.9429
F1-3	−0.898	0.9515
F2-1	−0.400	0.8984
F2-2	−0.571	0.8539

4. Discussion

An examination of numerical results proves that a revised model of the Equation (1) better presents the surface electrical resistivity of fiber-reinforced concrete:

$$R_{FRC} = R_{PC}e^{(pv\frac{\ell}{d}+q)}, \quad (4)$$

where R_{FRC} and R_{PC} are the measured electrical resistivity ($\Omega \cdot m$) of fiber-reinforced and plain concrete, respectively, ℓ is the fiber length (mm), d is the fiber diameter (mm), v is the volumetric fiber content (%), and p and q are regression constants. Figure 9 displays the curve fitting surface for measured data with R_{PC} of $1105 \Omega \cdot m$, and p and q are $-0.0214 \pm 2.02 \times 10^{-3}$ and $0.0556 \pm 2.70 \times 10^{-2}$ for 95% confidence bounds, respectively. The proposed fitted curve suggests that the reduction of surface electrical resistivity is negligible for small fiber contents, say 0.1%, or small aspect ratio, say two, disregarding other parameters (Figure 10). However, high fiber contents and large aspect ratios warrant an adjustment in the measured value using the proposed model. The error in predicted surface electrical resistivity is typically between -20 and 10% of the measured value for plain concrete (Figure 11). This range falls within the 21% tolerance for bias per standard methods [26]. Further, Figure 12 and Table 4 compares experimental values (Figure 1) and the numerical results of the presented study. This comparison qualitatively confirms the matching trends in reducing electrical resistivity with increasing fiber contents. The quantitative interpretation of results relies on the large tolerance specified by standard methods, like the specified 21% by AASHTO T 35 [26], considering the significant bias expected in experimental methods.

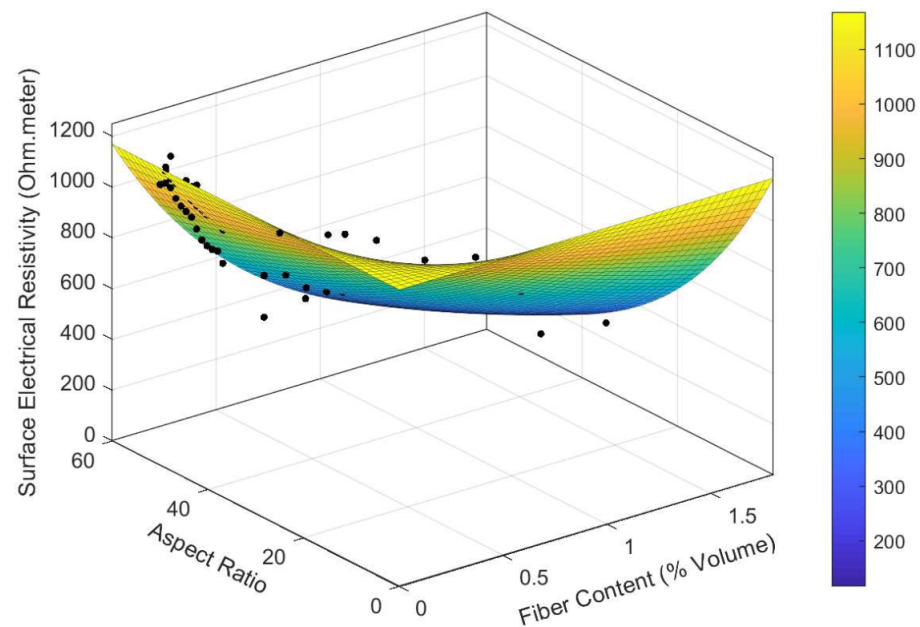


Figure 9. The electrical resistance for different percentages of fiber content.

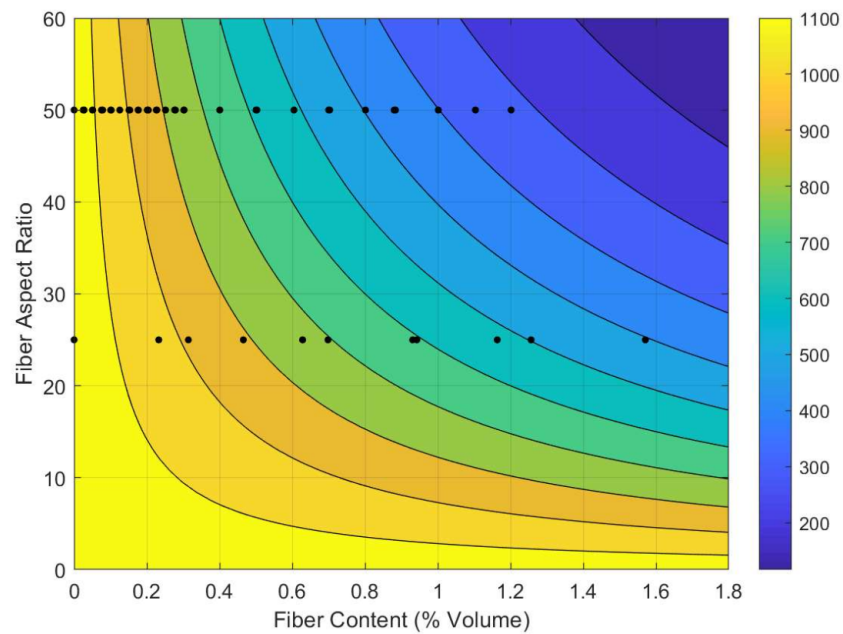


Figure 10. The surface electrical resistance ($\Omega \cdot m$) contour map for the proposed fit.

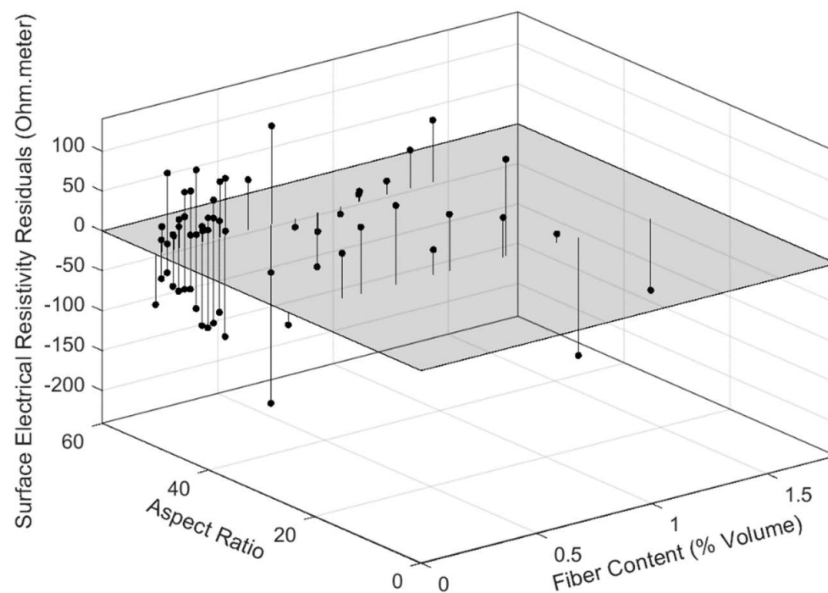


Figure 11. The residuals plot of surface electrical resistance ($\Omega \cdot m$) for the proposed fit.

Table 4. Formula of trends in (Figure 12).

Source	Exponential Rate of Decline	Coefficient of Determination
Cordon et al. (2020) [43]	-0.679	0.7606
Banthia et al. (1992) 1-day [49]	-0.371	0.9119
Banthia et al. (1992) 7-days [49]	-0.452	0.9275
Banthia et al. (1992) 28-days [49]	-0.461	0.9669
F1-1	-0.994	0.9789
F1-2	-1.47	0.9800
F1-3	-0.898	0.9752
F2-1	-0.45	0.9636
F2-2	-0.608	0.9035

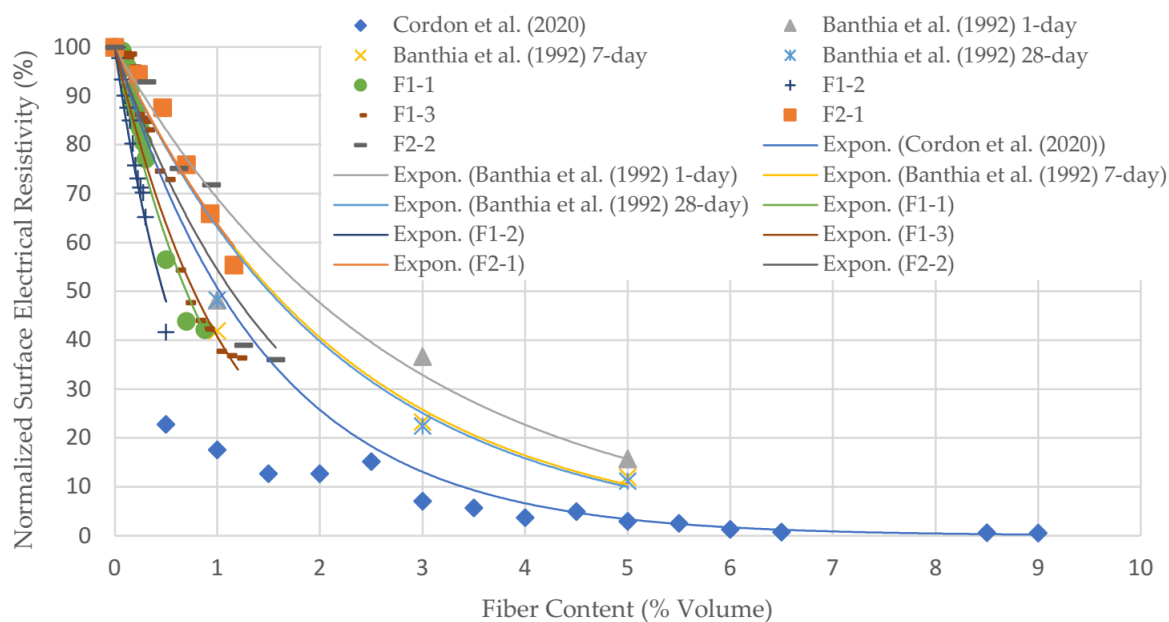


Figure 12. Comparison of the results of numerical and experimental experiments [43,49].

5. Conclusions

The conductivity of steel fibers influences the measured electrical resistivity of concrete. The number, length, and diameter of fibers interact to influence the electrical properties of fiber-reinforced concrete. Long fibers bridge over the cementitious matrix of concrete to transmit electrical current. Large diameters also increase the conductivity, making the effect of aspect ratio nontrivial. Further, the application of larger fibers in length or diameter reduces the total number of fibers at a constant fiber volume content.

Moreover, inherent uncertainties in the distribution of fibers throughout the concrete body warrant performing numerical simulations to address potential errors in experimental and practical measurements. Presented numerical simulations in this study indicated that aspect ratio and fiber volume contents could describe the surface electrical resistivity of fiber-reinforced concrete with an acceptable level of confidence. The proposed regression model incorporated improvements in the prediction equation.

Validation of presented results is limited to the availability of experimental results for verification purposes and computational challenges concerning the model dimensions. Hence, results warrant further studies to render comparisons with empirical data and broaden the range of parameters like the aspect ratio for extended model application.

Author Contributions: Conceptualization, F.M.T.; Methodology, F.M.T. and A.M.; Software, A.M.; Validation, A.M. and R.E.; Formal analysis, F.M.T., A.M. and R.E.; Investigation, F.M.T. and R.E.; Resources, F.M.T., A.M. and R.E.; Data curation, A.M.; Writing—original draft preparation, F.M.T., A.M. and R.E.; Writing—review and editing, F.M.T.; Visualization, F.M.T., R.E. and A.M.; Supervision, F.M.T.; Project administration, F.M.T. All authors have read and agreed to the published version of the manuscript.

Funding: This research received no external funding.

Institutional Review Board Statement: Not applicable.

Informed Consent Statement: Not applicable.

Data Availability Statement: All generated data are presented in this paper. No other data were created or analyzed in this study. Data sharing is not applicable to this article.

Acknowledgments: Authors acknowledge computer lab resources provided by their own affiliated institutes.

Conflicts of Interest: The authors declare no conflict of interest.

References

1. Tehrani, F.M.; Nelson, D. From Sustainability to Resilience: A Practical Guide to ENVISION[®]. In *Objective Resilience, Book 2: Objective Processes*; Ettouney, M., Ed.; ASCE Press: Reston, VA, USA, 2022.
2. Nelson, D.; Tehrani, F.M. Is resilience . . . sustainable? *APWA Rep.* **2018**, *85*, 53–56.
3. Tehrani, F.M. Deploying and Rating Sustainable Practices for Resilient Bridge Infrastructure. In Proceedings of the Fifth International Conference on Bridges, Tehran, Iran, 17–18 December 2019; AUT: Tehran, Iran, 2019; Paper MS05.
4. Tehrani, F.M.; Miller, N.M. Tire-Derived Aggregate Cementitious Materials: A Review of Mechanical Properties. In *Cement-Based Materials*; Saleh, H., Ed.; IntechOpen: London, UK, 2018.
5. Berry, E.; Shadravan, B.; Tehrani, F.M. A Sustainable Approach to Assess the Resilience of Perforated Wood Shear Walls. In Proceedings of the AEI Conference, Oklahoma City, OK, USA, 11–13 April 2017; ASCE: Reston, VA, USA, 2017; pp. 506–512.
6. Tehrani, F.M. Sustainability and Resilience through Project Management. In Proceedings of the 5th International Congress on Civil Engineering, Architecture & Urban Development, Tehran, Iran, 17–18 December 2017; AB-01440-B; ICSAU: Tehran, Iran, 2017.
7. Tehrani, F.M.; Dadkhah, M. A Case Study on the Analysis of Energy and Emissions for Sustainability Rating. *Int. J. Clim. Chang. Impacts Responses* **2018**, *10*, 13–23. [[CrossRef](#)]
8. Tehrani, F.M.; Alexandrou, A.; Mahoney, M.; Adhikari, D.; Raymond, M. Energy inputs and carbon dioxide emissions from construction equipment during construction of a golf course. *Int. J. Eng. Res. Innov.* **2014**, *6*, 78–86.
9. Kosmatka, S.H.; Kerkhoff, B.; Panarese, W.C. *Design and Control of Concrete Mixtures*; Portland Cement Association: Skokie, IL, USA, 2002.
10. Gulden, W. *Continuously Reinforced Concrete Pavement: Extending Service Life of Existing Pavements*; Report No. FHWA-HIF-13-024; Federal Highway Administration: Washington, DC, USA, 2013.
11. Tehrani, F.M.; Farshidpour, R.; Pouramini, M.; Mousavi, M.; Esfahani, A.N. Sustainability Rating of Lightweight Expanded Clay Aggregates Using Energy Inputs and Carbon Dioxide Emissions in Life-Cycle Analysis. In Proceedings of the Sixth International Symposium on Life Cycle Civil Engineering, Ghent, Belgium, 28–31 October 2018; Caspeepe, R., Taerwe, L., Frangopol, D.M., Eds.; CRC Press: Boca Raton, FL, USA, 2018; pp. 2989–2993.
12. Tehrani, F.M.; Nazari, M.; Truong, D.; Farshidpour, R. Sustainability of Tire-Derived Aggregate Concrete: A Case Study on Energy, Emissions, Economy, and Envision. In Proceedings of the International Conference on Sustainable Infrastructure 2019: Leading Resilient Communities through the 21st Century 2019, Los Angeles, CA, USA, 6–9 November 2019; Chester, M.V., Norton, M., Eds.; ASCE: Reston, VA, USA, 2019; pp. 399–408.
13. Nazari, M.; Tehrani, F.M.; Ansari, M.; Jeevanlal, B.; Rahman, F.; Farshidpour, R. *Green Strategies for Design and Construction of Non-Auto Transportation Infrastructure*; Report 19-17; Mineta Transportation Institute: San Jose, CA, USA, 2019.
14. Nazari, M.; Tehrani, F.M.; Ansari, M. Lightweight Rubberized Concrete Slabs for Sustainable Road Pavements Serving Non-Auto Traffic. *Period. Polytech. Civ. Eng.* **2022**. [[CrossRef](#)]
15. Davodijam, F.; Dastan Diznab, M.A.; Tehrani, F.M. Sustainability Rating of Internally-Cured Concrete in Marine Environments Using Service Life Prediction Models. In Proceedings of the ASCE International Conference on Sustainable Infrastructure 2021, Houston, TX, USA, 2–4 December 2021; ASCE: Reston, VA, USA, 2022; pp. 141–150.
16. Kalantari, S.; Dastan Diznab, M.A.; Tehrani, F.M. Sustainability of Internally-Cured Concrete for Mitigating Shrinkage Cracking Using Service Life Prediction Models. In Proceedings of the International RILEM Conference on Early-Age and Long-Term Crack Width Analysis in RC Structures, Paris, France, 9 April 2021; Kanavaris, F., Benboudjema, F., Azenha, M., Eds.; Springer: Cham, Switzerland, 2021; pp. 277–289.
17. Kalantari, S.; Tehrani, F.M. Enhancing the Resilience of Concrete Pavements Using Service Life Prediction Models. In Proceedings of the ASCE International Airfield & Highway Pavements Conference: Pavement Design Construction, and Condition Evaluation, Austin, TX, USA, 8–10 June 2021; Ozer, H., Rushing, J.F., Leng, Z., Eds.; ASCE: Reston, VA, USA, 2021; pp. 178–185.
18. Pouramini, M.; Tehrani, F.M. The Durability of High Strength Concrete Pavements Exposed to Freeze-Thaw Cycles in Different Saline Environments. In Proceedings of the ASCE International Airfield & Highway Pavements Conference: Pavement Design Construction, and Condition Evaluation, Austin, TX, USA, 8–10 June 2021; Ozer, H., Rushing, J.F., Leng, Z., Eds.; ASCE: Reston, VA, USA; pp. 159–168.
19. Bentz, D.P.; Clifton, J.R.; Ferraris, C.F.; Garboczi, E.J.; Torrents, J.M. *Transport Properties and Durability of Concrete: Literature Review and Research Plan*; NISTIR-6395; NIST: Washington, DC, USA, 1999.
20. Tehrani, F.M. Service Life Prediction of Internally Cured Concrete Pavements using Transport Properties. In Proceedings of the ASCE International Airfield & Highway Pavements Conference: Pavement Design Construction, and Condition Evaluation, Austin, TX, USA, 8–10 June 2021; Ozer, H., Rushing, J.F., Leng, Z., Eds.; ASCE: Reston, VA, USA, 2021; pp. 82–91.
21. Tehrani, F.M. *Service Life Prediction of Structural Lightweight Concrete Using Transport Properties*; ESCSI Report 4363; ESCSI: Chicago, IL, USA, 2020.
22. *ASTM C1556-11A*; Standard Test Method for Determining the Apparent Chloride Diffusion Coefficient of Cementitious Mixtures by Bulk Diffusion. American Society for Testing and Materials: West Conshohocken, PA, USA, 2016.

23. Azarsa, P.; Gupta, R. Electrical resistivity of concrete for durability evaluation: A review. *Adv. Mater. Sci. Eng.* **2017**, *2017*, 8453095. [[CrossRef](#)]
24. Layssi, H.; Ghods, P.; Alizadeh, A.R.; Salehi, M. Electrical resistivity of concrete. *Concr. Int.* **2015**, *37*, 41–46.
25. *ASTM C1876-19*; Standard Test Method for Bulk Electrical Resistivity or Bulk Conductivity of Concrete. American Society for Testing and Materials: West Conshohocken, PA, USA, 2019.
26. *AASHTO T358-19*; Standard Method of Test for Surface Resistivity Indication of Concrete's Ability to Resist Chloride Ion Penetration. American Association of State and Highway Transportation Officials: Washington, DC, USA, 2019.
27. Rupnow, T.D.; Icenogle, P.J. Surface resistivity measurements evaluated as alternative to rapid chloride permeability test for quality assurance and acceptance. *Trans. Res. Rec.* **2012**, *2290*, 30–37. [[CrossRef](#)]
28. Maraveas, C.; Bartzanas, T. Sensors for Structural Health Monitoring of Agricultural Structures. *Sensors* **2021**, *21*, 314. [[CrossRef](#)]
29. Tehrani, F.M. An Experimental Investigation of Mechanical Properties of Bonded Concrete. *Eur. J. Eng. Res. Sci.* **2020**, *5*, 88–91. [[CrossRef](#)]
30. Tehrani, F.M. Performance of Steel Fiber Reinforced Concrete in Beam-Column Connections. Ph.D. Thesis, University of California, Los Angeles, CA, USA, 2008.
31. Tehrani, F.M.; Serrano, R.M. Crack propagation of concrete beams prestressed with single strand tendons. *J. Civ. Eng. Res.* **2014**, *4*, 71–81.
32. Walraven, J.C. High performance fiber reinforced concrete: Progress in knowledge and design codes. *Mater. Struct.* **2009**, *42*, 1247–1260. [[CrossRef](#)]
33. Sivakumar, A.; Santhanam, M. Mechanical properties of high strength concrete reinforced with metallic and non-metallic fibres. *Cem. Concr. Compos.* **2007**, *29*, 603–608. [[CrossRef](#)]
34. McComb, C.; Tehrani, F.M. Enhancement of shear transfer in composite deck with mechanical fasteners. *Eng. Struct.* **2015**, *88*, 25–261. [[CrossRef](#)]
35. Rico, S.; Farshidpour, R.; Tehrani, F.M. State-of-the-art Report on Fiber-reinforced Lightweight-aggregate Concrete Masonry. *J. Adv. Civ. Eng.* **2017**, *2017*, 8078346. [[CrossRef](#)]
36. Soto, A.; Tehrani, F.M. An Investigation of Crack Propagation in Steel Fiber-Reinforced Composite Beams. *Period. Polytech. Civ. Eng.* **2018**, *62*, 956–962. [[CrossRef](#)]
37. Tehrani, F.M.; Rico, S.; Farshidpour, R. Shear Ductility of Fiber-Reinforced Lightweight-Aggregate Concrete Masonry. In Proceedings of the 11th US National Conference on Earthquake Engineering, Los Angeles, CA, USA, 25–29 June 2018; EERI: Oakland, CA, USA, 2018; p. 1112.
38. Mohammadi, Y.; Singh, S.P.; Kaushik, S.K. Properties of steel fibrous concrete containing mixed fibres in fresh and hardened state. *Constr. Build. Mater.* **2008**, *22*, 956–965. [[CrossRef](#)]
39. Klyuev, S.V.; Khezhev, T.A.; Pukharenko, Y.V.; Klyuev, A.V. Fiber concrete for industrial and civil construction. *Mater. Sci. Forum* **2019**, *945*, 120–124. [[CrossRef](#)]
40. Afroughsabet, V.; Ozbakkaloglu, T. Mechanical and durability properties of high-strength concrete containing steel and polypropylene fibers. *Constr. Build. Mater.* **2015**, *94*, 73–82. [[CrossRef](#)]
41. Bae, Y.; Pyo, S. Effect of steel fiber content on structural and electrical properties of ultra high performance concrete (UHPC) sleepers. *Eng. Struct.* **2020**, *222*, 111131. [[CrossRef](#)]
42. Payakaniti, P.; Pinitsoontorn, S.; Thongbai, P.; Amornkitbamrung, V.; Chindaprasirt, P. Electrical Conductivity and Compressive Strength of Carbon Fiber Reinforced Fly Ash Geopolymeric Composites. *Constr. Build. Mater.* **2017**, *135*, 164–176. [[CrossRef](#)]
43. Cordon, H.C.F.; Tadini, F.B.; Akiyama, G.A.; de Andrade, V.O.; da Silva, R.C. Development of electrically conductive concrete. *Cerâmica* **2020**, *66*, 88–92. [[CrossRef](#)]
44. Sanchez, J.; Andrade, C.; Torres, J.; Rebollo, N.; Fulla, J. Determination of reinforced concrete durability with on-site resistivity measurements. *Mater. Struct.* **2017**, *50*, 41. [[CrossRef](#)]
45. Lim, Y.C.; Noguchi, T.; Cho, C.G. A quantitative analysis of the geometric effects of reinforcement in concrete resistivity measurement above reinforcement. *Constr. Build. Mater.* **2015**, *83*, 189–193. [[CrossRef](#)]
46. Miri, A.; Ehsani, R.; Tehrani, F.M. A Numerical Simulation of the Electrical Resistivity of Concrete Pavements Containing Steel Fibers. In Proceedings of the ASCE International Airfield & Highway Pavements Conference: Pavement Design Construction, and Condition Evaluation, Austin, TX, USA, 8–10 June 2021; Ozer, H., Rushing, J.F., Leng, Z., Eds.; ASCE: Reston, VA, USA, 2021; pp. 356–364.
47. Lee, C.Y.; Wang, S.R. Analysis of resistance characteristics of conductive concrete using press-electrode method. *World Acad. Sci. Eng. Technol.* **2010**, *72*, 91–94.
48. Tuan, C.Y. *Implementation of Conductive Concrete for Deicing (Roca Bridge)*; Report SPR-P1(04) P565; NE Department of Transportation Research: Omaha, NE, USA, 2008.
49. Banthia, N.; Djeridane, S.; Pigeon, M. Electrical resistivity of carbon and steel micro-fiber reinforced cements. *Cem. Concr. Res.* **1992**, *22*, 804–814. [[CrossRef](#)]
50. You, I.; Yoo, D.Y.; Kim, S.; Kim, M.J.; Zi, G. Electrical and self-sensing properties of ultra-high-performance fiber-reinforced concrete with carbon nanotubes. *Sensors* **2017**, *17*, 2481. [[CrossRef](#)] [[PubMed](#)]
51. Butler, S.L.; Sinha, G. Forward modeling of applied geophysics methods using COMSOL and comparison with analytical and laboratory analog models. *Comput. Geosci.* **2012**, *42*, 168–176. [[CrossRef](#)]

-
52. Clement, R.; Bergeron, M.; Moreau, S. COMSOL: Multiphysics Modelling for Measurement Device of Electrical Resistivity in Laboratory Test Cell. In Proceedings of the 2011 COMSOL Conference, Stuttgart, Germany, 26–28 October 2011; COMSOL, Inc.: Burlington, MA, USA, 2011.
 53. COMSOL. *COMSOL Multiphysics 5.5 (Build: 359)*; COMSOL, Inc.: Burlington, MA, USA, 2019.
 54. MATLAB. *MATLAB and Statistics Toolbox Release 2021a*; The MathWorks, Inc.: Natick, MA, USA, 2021.
 55. Ruan, T.; Poursae, A. Fiber-distribution assessment in steel fiber-reinforced UHPC using conventional imaging, X-ray CT scan, and concrete electrical conductivity. *J. Mater. Civ. Eng.* **2019**, *31*, 04019133. [[CrossRef](#)]